Nanotechnology, Science and Applications

Dovepress
Taylor & Francis Group

Open Access Full Text Article

ORIGINAL RESEARCH

Guiding Cell Growth: Graphene-Patterned Polymeric Substrates for Enhanced Tissue Proliferation

Weronika Sosnowicz[1,2], Jakub Krzeminski[2], Jan Dominiczak[1,2], Dominik Baraniecki[1,2], Paulina Trzaskowska[2], Marta C Corvo[3], Zuzanna Żołek-Tryznowska[1], Arkadiusz Jeznach[1], Malgorzata Jakubowska[1,2], Lucja Dybowska-Sarapuk[1,2]

[1]Faculty of Mechanical and Industrial Engineering Warsaw University of Technology, Warsaw, 02-524, Poland; [2]Centre for Advanced Materials and Technologies CEZAMAT, Warsaw University of Technology, Warsaw, 02-822, Poland; [3]Department of Materials Science, CENIMAT|i3N, School of Science and Technology, NOVA University, Caparica, 2829-516, Portugal

Correspondence: Lucja Dybowska-Sarapuk, Faculty of Mechanical and Industrial Engineering Warsaw University of Technology, Ludwika Narbutta 85, Warsaw, 02-524, Poland, Email lucja.sarapuk@pw.edu.pl

Introduction: In tissue engineering, there is a growing need for patient-specific strategies that enable precise control of cellular behaviour — such as adhesion, proliferation, and migration — to enhance tissue integration and reduce transplant rejection. Engineering the physicochemical properties and topography of substrates is a promising way to guide cell responses. Among available materials, graphene nanoplatelets offer outstanding physicochemical, electrical, and mechanical properties, making them ideal for biomedical use. Moreover, printed electronics techniques allow efficient, cost-effective fabrication of continuous coatings or intricate micropatterns on flexible substrates.

Methods: Graphene nanoplatelet patterns were fabricated on flexible thermoplastic polyurethane substrates using inkjet and aerosol jet printing to compare the methods and their influence on cell behaviour. Layers were analysed for morphology, topography, and electrical properties (SEM, Raman spectroscopy, profilometry, electrical measurements). Surface wettability and surface free energy were measured via contact angle measurements. L929 fibroblast cells were cultured on printed patterns and assessed by confocal microscopy and MTT assay.

Results and Discussion: Graphene patterns significantly improved cell proliferation compared to TPU controls. Cells aligned and migrated along printed graphene features, especially on aerosol jet-printed patterns, which promoted attachment and spreading. Quantitative analysis confirmed enhanced cell coverage and proliferation, highlighting the potential of graphene micropatterns for precise cellular control in regenerative medicine.

Keywords: graphene patterning, cell guidance, tissue engineering, ink-jet printing, aerosol jet printing, graphene nanoplatelets

Introduction

One of the goals of today's regenerative engineering is to develop artificial biological systems with tailored properties that allow integration into cells.[1,2] Modifying stem cell growth and proliferation is essential in various biomedical applications. Multiple types of materials are increasingly being explored in the field of personalized medicine.[3–5] Polymer composites are widely used in tissue engineering due to their low cost, the ability to modulate material properties, the possibility of complete personalization, and the ease of functionalizing materials.[6–8]

Tissue engineering aims to develop highly flexible, mechanically robust materials that provide a conductive environment for cell growth. Nanomaterials, particularly graphene derivatives, have garnered significant attention due to their unique physicochemical properties, thus enabling them to overcome biological barriers. Their nanoscale dimensions, similar to the constituents of extracellular matrices forming tissue structures, make graphene materials highly effective as cell substrates and scaffolds.[7,9,10] Graphene/polymer composites are widely used in biomedical applications, including drug

Received: 29 March 2025
Accepted: 19 August 2025
Published: 14 November 2025

delivery systems, sensors, and the production of 3D scaffolds and culture substrates.[4] Graphene's unique properties make it highly promising in biologically active cellular scaffolds and regenerative medicine strategies, especially when combined with biopolymers and composites.[11,12] A wide range of physicochemical properties and ease of functionalization encourages the increasing use of graphene materials as composite fillers, scaffolds, and cell substrates, while providing an effective interface between the substrate and the culture system.[5,13–16] Due to their developed chemical structure, graphene materials induce the attachment of molecules and particles responsible for cell adhesion to the substrate, patterning, or migration. The high flexibility of graphene materials enables the preparation of adaptable structures with adjustable stiffness moduli. This property allows the matching of specific injury sites, damaged tissue, or implants, paving the way to a more efficient and cost-effective approach to repairing damaged nerves or spinal cords.[5] Numerous studies have explored the application of graphene oxide (GO) and reduced graphene oxide (rGO) in cell culture and stem cell differentiation.[17–20] Owing to the presence of abundant oxygen-containing functional groups on their surfaces, GO and rGO exhibit superior functionalization capacity compared to other graphene-based materials. Additionally, their inherent hydrophilicity—a highly desirable property in biological contexts—facilitates their dispersion in aqueous media, broadening their applicability in biomedical systems. However, despite these advantages, both GO and rGO demonstrate significantly lower electrical conductivity and mechanical strength compared to graphene nanoplatelets (GNPs).[21] These limitations reduce their effectiveness as scaffold materials for applications involving electrical stimulation, where efficient charge transfer and mechanical integrity are critical.[22] Even when eco-friendly reducing agents, such as L-ascorbic acid, are employed to improve their conductivity, the resultant materials still fall short in delivering consistent and efficient electroactive performance.[22] Consequently, while GO and rGO remain valuable for certain biomedical applications, their utility in electroconductive scaffolding for neural tissue engineering is comparatively limited.[23] GO generally exhibits a higher degree of oxidation, which not only reduces its electrical conductivity but may also increase its potential cytotoxicity.[24] Graphene nanoplatelets (GNP) are distinguished by their flat, platelet-like structure which provides not only conductive properties and a large surface but also mechanical reinforcement area beneficial for surface interactions, making them particularly suitable for cell culture studies.[25] However, the large specific surface area of GNP results in electrostatic van der Waals forces and strong π-π interplanar interactions. Consequently, this leads to the formation of GNP agglomerates, which limit the electrical and mechanical properties of polymer composites, thereby hindering the manufacturing of high- quality composites.[11] To mitigate this phenomenon, optimizing the ink formulation by carefully selecting appropriate constituents is imperative. This includes the precise determination of solvent, functional phase polymers, and when necessary – the incorporation of surface-active agents or other rheology modifiers.[26–28] The synergistic interaction of these components must be tailored to achieve the desired physicochemical properties, such as surface tension, viscosity, and drying kinetics, which are critical for preventing printing artifacts like the coffee ring effect and ensuring a uniform deposition of the functional material.[29,30] Graphene/polymer composites are widely used in biomedical applications, including drug delivery systems, sensors, and the production of 3D scaffolds and culture substrates.[4] Graphene's unique properties make it highly promising in biologically active cellular scaffolds and regenerative medicine strategies, especially when combined with biopolymers and composites.[11,12] A wide range of physicochemical properties and ease of functionalization encourages the increasing use of graphene materials as composite fillers, scaffolds, and cell substrates, while providing an effective interface between the substrate and the culture system.[5,13–16] Due to presence of functional groups, graphene materials induce the attachment of molecules and particles responsible for cell adhesion to the substrate, patterning, or migration. The high flexibility of graphene materials enables the preparation of adaptable structures with adjustable stiffness moduli. This property allows the matching of specific injury sites, damaged tissue, or implants, paving the way to a more efficient and cost-effective approach to repairing damaged nerves or spinal cords.[5] Numerous studies have explored the application of graphene oxide (GO) and reduced graphene oxide (rGO) in cell culture and stem cell differentiation.[17–20] Owing to the presence of abundant oxygen-containing functional groups on their surfaces, GO and rGO exhibit superior functionalization capacity compared to other graphene-based materials. Additionally, their inherent hydrophilicity—a highly desirable property in biological contexts—facilitates their dispersion in aqueous media, broadening their applicability in biomedical systems. However, despite these advantages, both GO and rGO demonstrate significantly lower electrical conductivity and mechanical strength compared to graphene nanoplatelets (GNPs).[21] These limitations reduce their effectiveness as scaffold materials for applications involving electrical stimulation, where efficient

charge transfer and mechanical integrity are critical.[22] Even when eco-friendly reducing agents, such as L-ascorbic acid, are employed to improve their conductivity, the resultant materials still fall short in delivering consistent and efficient electroactive performance.[22] Consequently, while GO and rGO remain valuable for certain biomedical applications, their utility in electroconductive scaffolding for neural tissue engineering is comparatively limited.[23] GO generally exhibits a higher degree of oxidation, which not only reduces its electrical conductivity but may also increase its potential cytotoxicity.[24] Graphene nanoplatelets (GNP) are distinguished by their flat, platelet-like structure which provides not only conductive properties and a large surface but also mechanical reinforcement area beneficial for surface interactions, making them particularly suitable for cell culture studies.[25] However, the large specific surface area of GNP results in electrostatic van der Waals forces and strong π-π interplanar interactions. Consequently, this leads to the formation of GNP agglomerates, which limit the electrical and mechanical properties of polymer composites, thereby hindering the manufacturing of high- quality composites.[11] To mitigate this phenomenon, optimizing the ink formulation by carefully selecting appropriate constituents is imperative. This includes the precise determination of solvent, functional phase polymers, and when necessary – the incorporation of surface-active agents or other rheology modifiers.[26–28] The synergistic interaction of these components must be tailored to achieve the desired physicochemical properties, such as surface tension, viscosity, and drying kinetics, which are critical for preventing printing artifacts like the coffee ring effect and ensuring a uniform deposition of the functional material.[29,30]

The substrate also plays a critical role in cell culture studies. Mainly, the objective is to ensure high cell adhesion to the substrate, which is heavily dependent on the chemical structure of the selected material. Cell-substrate interactions generally depend on the substrate's surface free energy (SFE) and its polar and nonpolar components.[4] Every surface has its characteristic SFE, reflecting its attraction capacity and determining specific properties such as hydrophilicity and hydrophobicity.[31,32] A thorough analysis of SFE is essential to predict the material's behaviour during interactions. Several surface modification methods can be applied to increase the SFE, such as plasma, corona, or flame treatment. These methods disrupt the polymer's long chains while increasing the number of available polar group bonds (–OH, –C=O, –COOH).[33,34] Polar groups on the substrate's surface promote chemical interactions and bond formation between the substrate and the cell membrane, resulting in strong adhesion. Numerous studies have investigated the effects of surface free energy on cellular adhesion to substrates utilizing glass, metal, or standard culture plastic substrates while proving that cell behaviour may also be affected by surface roughness.[2,32,34–36] Therefore, new substrates for tissue engineering are highly sought after, including printed layers of graphene-based materials. Due to the high specific surface area, graphene materials can create rough pathways that guide cell migration, stimulate proliferation, and induce differentiation of cells into particular phenotypes.[37]

Recent studies demonstrate numerous printing techniques employed to produce micropatterned pathways. Methods such as soft photolithography, electron beam lithography, stamping/impression, or etching are most often used as well-established techniques in the field.[18,38,39] However, these techniques have disadvantages, which include the preparation of technologically complex molds and masks, resulting in relatively high production costs and prolonged preparation time due to multiple manufacturing processes being used. Moreover, the utilization of highly toxic materials typical for the etching processes is both an environmental hazard as well as a health risk to the operators.[40,41] Recent studies propose printed electronics techniques as an alternative to those mentioned above. Ink-jet printing (IJP) and aerosol-jet printing (AJP) have gained considerable attention in tissue engineering. These microprinting techniques allow for the manufacturing of tailor-made structures while considering the development of sustainable solutions and the use of environmentally friendly materials. As both techniques utilize drop-on-demand systems, they allow for low material consumption, waste reduction and lowered production costs.[42,43] Although both techniques use liquid ink containing functional material (eg GNP) that is deposited on the substrate through the nozzle, they differ regarding printing process. IJP utilizes thermal or ultrasonic actuation to eject a droplet typically ranging in 20–50 μm diameter which results typically in up to 100 μm dot on the substrate.[44] In AJP ink is atomized to the aerosol mist of droplets (1–5 μm in diameter) and transported in a gas flow –deposited dot may be even under 10 μm in diameter.[45]

Several studies report using IJP and AJP printed graphene substrates in cell culture. The high printing resolution of just a few micrometres and deposition method allowing for an effective specific surface area distinguish these techniques from other printed electronics techniques.[43,46–48] Although no reports describing the use of AJP for printing graphene

substrates have been found, there are works showing application of AJP in the field of cell culture. These includes successful fabrication of biocompatible carbon-based impedance sensor for continuous monitoring of scaffold-based cultures, spatial scaffolds made from collagen composite ink for bone tissue engineering and silver RC circuits – pulse generators designed for electrical stimulation in neural tissue engineering.[41,49,50] A similar situation is observed for IJP. While the literature predominantly reports its use for biopolymer printing, no studies have been identified that employ graphene nanoplatelets specifically for guiding cell attachment and migration.[47,48] Nevertheless, there are documented applications of various graphene-based materials in the printing of biosensors and electrodes designed for the monitoring of cell cultures.[6,51] While both deposition techniques have been previously investigated, there is a notable lack of research comparing their respective advantages and disadvantages for fabricating cell culture substrates. Moreover, despite extensive investigations into the use of graphene materials in cell culture studies, these predominantly focus on graphene oxides and reduced forms of graphene.[6,42,52] These materials, while dispersible in water due to the presence of oxygen functionalities, lack the electrical conductivity and mechanical robustness that are hallmark properties of graphene.[18,53] In contrast, the use of GNP represents a novel approach in this field. GNP retain the intrinsic electrical and mechanical properties of graphene. This innovation highlights the potential of GNP-based substrates to address the limitations of graphene oxides, presenting a significant advancement in the development of high-performance cell culture platforms. While both deposition techniques have been previously investigated, there is a notable lack of research comparing their respective advantages and disadvantages for fabricating cell culture substrates. Moreover, despite extensive investigations into the use of graphene materials in cell culture studies, these predominantly focus on graphene oxides and reduced forms of graphene.[6,42,52] These materials, while dispersible in water due to the presence of oxygen functionalities, lack the electrical conductivity and mechanical robustness that are hallmark properties of graphene.[18,53] In contrast, the use of GNP represents a novel approach in this field. GNP retain the intrinsic electrical and mechanical properties of graphene. This innovation highlights the potential of GNP-based substrates to address the limitations of graphene oxides, presenting a significant advancement in the development of high-performance cell culture platforms. Although no reports describing the use of AJP for printing graphene substrates have been found, there are works showing application of AJP in the field of cell culture. These includes successful fabrication of biocompatible carbon-based impedance sensor for continuous monitoring of scaffold-based cultures, spatial scaffolds made from collagen composite ink for bone tissue engineering and silver RC circuits – pulse generators designed for electrical stimulation in neural tissue engineering.[41,49,50] A similar situation is observed for IJP. While the literature predominantly reports its use for biopolymer printing, no studies have been identified that employ graphene nanoplatelets specifically for guiding cell attachment and migration.[47,48] Nevertheless, there are documented applications of various graphene-based materials in the printing of biosensors and electrodes designed for the monitoring of cell cultures.[6,51] While both deposition techniques have been previously investigated, there is a notable lack of research comparing their respective advantages and disadvantages for fabricating cell culture substrates. Moreover, despite extensive investigations into the use of graphene materials in cell culture studies, these predominantly focus on graphene oxides and reduced forms of graphene.[6,42,52] These materials, while dispersible in water due to the presence of oxygen functionalities, lack the electrical conductivity and mechanical robustness that are hallmark properties of graphene.[18,53] In contrast, the use of GNP represents a novel approach in this field. GNP retain the intrinsic electrical and mechanical properties of graphene. This innovation highlights the potential of GNP-based substrates to address the limitations of graphene oxides, presenting a significant advancement in the development of high-performance cell culture platforms. While both deposition techniques have been previously investigated, there is a notable lack of research comparing their respective advantages and disadvantages for fabricating cell culture substrates. Moreover, despite extensive investigations into the use of graphene materials in cell culture studies, these predominantly focus on graphene oxides and reduced forms of graphene.[6,42,52] These materials, while dispersible in water due to the presence of oxygen functionalities, lack the electrical conductivity and mechanical robustness that are hallmark properties of graphene.[18,53] In contrast, the use of GNP represents a novel approach in this field. GNP retain the intrinsic electrical and mechanical properties of graphene. This innovation highlights the potential of GNP-based substrates to address the limitations of graphene oxides, presenting a significant advancement in the development of high-performance cell culture platforms.

Below, we demonstrate a novel approach for enhancing the structural organization of L929 cells. We performed a comparison of ink-jet printing and aerosol-jet printing as manufacturing methods of graphene substrates for cell culture by characterization of the morphology and the chemical structure of the printed micropatterns. As we aimed to take advantage of the conductive properties of graphene, we resolved to utilize an ink based on graphene nanoplatelets as a material with properties akin to pure graphene. In our study, we introduced an innovative approach to creating substrates to explore the impact of graphene micropatterning on cell behaviour. Microarrays of lines and grids produced in the study significantly affected cells attachment and migration.

Materials and Methods

Fabrication of Graphene Patterns on TPU Substrates

In this work, commercial graphene ink GNP-AJ-00 from Novelinks Ltd. (Novelinks Sp. z o.o. Poland) was used. The product was developed in collaboration with Novelinks Ltd. for microprinting technology applications. The ink based on graphene nanoplatelets (with a size of 2 μm, an average thickness of 8–15 nm, and a Specific Surface Area of 500–700 m2/g) dispersed in a polymer matrix and solvents was used to produce the patterns. The formulation demonstrated sufficient colloidal stability for several hours, enabling reliable printing without significant sedimentation of the graphene particles during the process. Nevertheless, to ensure optimal homogeneity and prevent potential agglomeration, the ink was homogenized for 30 minutes in an ultrasonic bath before each printing session.

A 0.127 mm thick thermoplastic polyurethane (TPU) film produced by Adhesive films (USA) was applied as the substrate. The film underwent heating in a laboratory dryer at 120°C for 30 minutes to eliminate the stresses present in its structure. Prepared substrates were employed for printing patterns using two microprinting technologies: ink-jet printing and aerosol-jet printing. For IJP printing the Microdrop Dispenser Head MD-K-130 (Microdrop Technologies GmbH, Germany) with 70 μm inner nozzle diameter was used, operating in drop-on demand mode. No table heating was used during the printing process. For AJP printing an Optomec Aerosol Jet Printer with a 100 μm nozzle was used. Lines and grids, at three distinct resolutions were prepared. Prints were executed in lines and grids at distances of 2, 1, and 0.5 mm. The layers were dried in a Memmert UF55 laboratory dryer with natural air circulation (Memmert GmbH & Co. KG; Schwabach, Germany) in 120 °C for 15min. The printing parameters for IJP and AJP are presented in Tables 1 and 2 below.

Characterization of the Prints

A UNI-T laboratory multimeter, model UT804 (Uni-Trend Technology, Co., Ltd.; Shanghai, China), was used to measure the resistance of the fabricated coatings. The thickness and surface area of the layers were measured with the DektakXT Bruker BNS stylus profilometer with 12.5mm radius tip. The results were analysed using Vision64 software from Bruker. Macrogeometry of the prints was observed using the Keyence VHX-900F and VHX-X1 digital microscopes (Keyence International (Belgium), NA/SA; Mechelen, Belgium) with VH-Z20R and VHX-E500 lenses. 20 print samples were made for each printing technique. Measurement uncertainties are given as the standard deviation from the mean of the measurements.

Characterization SEM Analysis, Raman and EDS studies: a Hitachi SU8230 scanning electron microscope (SEM) was used to evaluate the structure of the printed patterns. In the registration, an accelerating voltage of 15kV was used. The samples were sputtered with a Quorum QT150 S laboratory sputtering machine using a 60:40 Au:Pd alloy target before SEM

Table 1 Ink-Jet Printing Parameters

Voltage [V]	Width [ms]	Frequency [Hz]	Dwell Time [ms]	Velocity [mm/s]	Acceleration [mm/s^2]
80	45	55	500	10	10

Table 2 Aerosol Jet Printing Parameters

Sheath Flow [sccm]	Atomization Flow [sccm]	Exhaust Flow [sccm]	Platen Temp. [°C]	Velocity [mm/s]
50	560	760	60	10

Table 3 Measurements of Water and Diiodomethane Contact Angle (°), and Surface Free Energy (Es) of the Different Graphene and TPU Film Surfaces

Sample	Diiodomethane Contact Angle (°)	Water Contact Angle (°)	Surface Free Energy (mJ/m^2)		
			Total	Dispersive	Polar
TPU film without heating	51.3	88.9	35.6	33.6	1.9
TPU film with heating in 120 °C for 30 min	60.9	84.2	32.7	28.0	4.6
Graphene layer	39.9	87.3	42.6	41.3	1.2

examination. An EDS system with a Bruker XFlash 7 setup was used to analyze the elemental composition of the printed structures. When comparing elemental composition, the focus was on analyzing carbon and oxygen content. Peaks from gold (Au), palladium (Pd), silicon (Si) and Aluminum (Al) were omitted because they originated from the sputtered layer and the substrate material. Raman spectroscopy measurements were performed in a Renishaw inVia Reflex micro-Raman spectrometer (Renishaw plc, Wotton-under-Edge, UK) equipped with an air-cooled CCD detector and a HeNe laser operating at 50 mW of 532 nm laser excitation. The spectral resolution of the spectroscopic system was 0.3 cm−1. The laser beam was focused with a 100x Leica objective lens (N Plan EPI, Leica Microsystems, Wetzlar, Germany) with a numerical aperture of 0.75. An integration time of 10s was used for all measurements, and the intensity of the incident laser was 2.5 mW. Spectra were obtained in triplicate for each sample at room temperature in the wavelength range between 1000 and 3500 cm−1.

Surface Free Energy and Wettability Measurements

The surface free energy was measured using the Drop Shape Analyzer DSA30E (Krüss, Germany). The experimental procedure involved applying droplets of water and diiodomethane onto the surfaces under investigation using a needle with a diameter of 0.5 mm. Subsequently, the shape of the obtained droplets underwent detailed digital analysis. The surface free energy and the polar and nonpolar components were determined according to the Owens-Wendt method. The measurement error of the wetting angle was ± 1.0 degree. Measurements of water and diiodomethane contact angle (°) and surface free energy (Es) of the different graphene and TPU film surfaces are presented in the Table 3.

Cell Sample and Substrate Preparation

L929 mouse adipose tissue-derived fibroblast cells (Sigma Aldrich, 85011425, mouse C3H/An connective tissue) were precultured in cell culture incubator set at 37 °C with 5% CO2, following the manufacturer's instructions. Cells derived from passages 3–6 were utilized in this study. Dulbecco's Modified Eagle Medium (DMEM) (Gibco, Thermo Fisher) was supplemented with 1% Glutamax (Thermo Fisher), 1% Penicillin-Streptomycin (Gibco, Thermo Fisher), and 10% Fetal Bovine Serum (FBS) (Thermo Fisher, USA). The 12 variants of the materials were used for cell studies, with 2 replicates for each time point (24 h and 72 h). Before seeding, substrates were sterilized as follows: substrates were transferred to sterile culture wells (24-well plate), then 0.5 mL of 70% ethanol was added to each well. After 30 min, the substrates were rinsed with Phosphate Buffered Saline (PBS) solution transferred to a new sterile well plate and thoroughly washed in PBS three times. L929 cells were cultured until reaching 80–90% confluence, then trypsinized and suspended in the supplemented medium, as mentioned above. Materials were seeded with the cells at a concentration of 1×105 cells/mL. Cultures were conducted for 24h and 72h. At these timepoints the cells were fixed and stained to allow observation with a confocal microscope according to the procedure described below in 1.7.

L929 Fixation and Fluorescence Staining

The cells were fixed in 4% paraformaldehyde for 15 minutes at room temperature, followed by rinsing with PBS on a laboratory shaker. Cell membranes were then permeabilized using a 0.2% solution of Triton X-100 in PBS (Sigma) for 8 minutes at room temperature on the laboratory shaker. Washing was again carried out in PBS on a laboratory shaker (3x5 minutes). The cells prepared in this manner were stained according to the following procedure: the first step involved blocking with 0.1% bovine serum albumin (BSA) for 90 minutes at room temperature. Subsequently, the actin

filaments of the cytoskeletons were stained with AlexaFluor488 antibody (Thermofisher) diluted according to manufacturer's instructions (300 µL of AlexaFluor488 per sample); the staining process lasted 1 hour in the dark. The final step was rinsing again in PBS on a shaker (3x5 minutes).

Visualization and analysis of L929 cells: The cells on the printed substrates were observed using a Zeiss LSM 880 confocal microscope using both fluorescence and transmission light mode. Each material variant was imaged at 5 different locations on the substrate with x100 magnification using a x10 magnification lens and x10 eyepiece.

MTT Assay

An MTT assay was prepared to evaluate the cytotoxicity of GNP prints. To further assess the potential cytotoxicity of the employed materials, additional graphene substrates were prepared, with 1 and 5 layers of Graphene ink. TPU foils were spraycoated with the same ink used in both AJP and IJP, thereby enabling evaluation of material biocompatibility even at elevated graphene loadings. The patterned substrates were prepared, as described in "Cell Sample and Substrate preparation" section.

To evaluate the potential cytotoxicity of the GNP prints, an indirect extract-based cytotoxicity assay was conducted in accordance with ISO 10993–5 and ISO 10993–12 standards. The assay was performed using the L929 mouse fibroblast cell line. Extracts were prepared based on surface area exposure (1 mL of extraction medium per 3 cm^2 of material).

Samples were first sterilized under a laminar flow hood using 70% ethanol for 30 minutes, followed by three washes with sterile DPBS. The sterilized samples were then immersed in complete Dulbecco's Modified Eagle Medium (DMEM) without phenol red, supplemented with 10% fetal bovine serum (FBS), 2 mM L-glutamine, 100 U/mL penicillin, and 100 µg/mL streptomycin. The extraction was carried out at 37°C in a humidified CO_2 incubator equipped with a shaker for 72 hours to allow the release of potential leachable. Each material type was extracted in triplicate.

Meanwhile, L929 fibroblast cells were seeded into a 96-well culture plate at a density of 1×10^4 cells/well in the same complete DMEM medium (without phenol red). After 24 hours of incubation to allow cell attachment, the culture medium was replaced with 100 µL of the respective extracts. Each extract was added in duplicate.

A 0.01% Triton X-100 solution in complete DMEM served as the positive control (PC), while complete DMEM (supplemented as above) served as the negative control (NC).

After 24 hours of exposure to the extracts, the MTT assay was performed. A volume of 10 µLof MTT solution (5 mg/mL in supplemented DMEM) was added to each well and incubated for 4 hours at 37°C. Formazan crystals formed by metabolically active cells were then solubilized using 10% SDS. Absorbance was measured at 570 nm using a microplate reader. Cell viability was expressed as the mean percentage relative to the negative control (% NC), with values above 70% considered non-cytotoxic. Standard deviations were calculated for each % NC.

Statistical Analysis

All quantitative results are reported as mean ± standard deviation (SD). Normality of residuals was assessed with the Shapiro–Wilk test ($\alpha = 0.05$). One-factor comparisons between printing techniques (AJP vs IJP; $n = 20$ per group) were made with a one-way ANOVA. Because the F-test is robust to moderate non-normality when sample sizes are equal, the ANOVA was retained; its outcome was verified with the non-parametric Mann–Whitney *U*-test. Significant ANOVA results were followed by Tukey's honestly significant difference (HSD) post-hoc contrasts. A two-sided $p < 0.05$ was considered statistically significant. Resistivity distributions were right-skewed and failed normality (Shapiro–Wilk, all $p < 0.01$); therefore, differences between techniques were assessed with the two-tailed Mann–Whitney *U*-test ($\alpha = 0.05$). For completeness, Welch's unequal-variance *t*-test was performed on $\log_{10}$-transformed data; both approaches led to the same conclusion. Effect size was expressed as the rank-biserial correlation. All analyses were performed in JASP v0.19.3 (JASP Team, 2025).

Results and Discussion

Preparation of the Printing Process and Cell Culture Substrates

In this study, we aimed to investigate the interaction between L929 cells and patterns made with GNP, which closely approximate graphene in terms of physicochemical properties. Therefore, a GNP-based ink was selected for examination.

The printing process required the optimalization of the printing parameters for both IJP and AJP. For IJP, the parameter selection process involved optimizing the following parameters: control voltage, signal width, droplet generation frequency, table movement speed and acceleration, and standstill time between successive layer deposition. The chosen parameters are presented in Table 1 of the Experimental Section. AJP requires the determination of working gas flows utilizing pneumatic atomization (Sheath Flow – SF, Atomization Flow – AF, Exhaust Flow – ExhF), heated platen temperature, table movement velocity and the number of printed layers. Recommended printing parameters for AJP are presented in Table 2 of the Experimental Section.

To ensure the suitability of the prints for cell culture applications, it was crucial to confirm their cytocompatibility, verify the adhesion to the substrate and check the stability under aqueous physiological conditions (such as phosphate-buffered saline and cell culture medium) as well as in ethanol, which is used for media sterilization prior to cell seeding.

Therefore, we conducted immersion tests on the substrates with printed patterns to simulate culture conditions. The tests included washing with ethanol and saline, followed by a 2-week immersion in DMEM. All tested samples were resistant to washing in the liquids, with no observable delamination or redispersion. The prints maintained their integrity without dissolution, exhibited unchanged adhesion to the substrate post-test, and no particulate matter was detected in the immersion liquid.

Wettability of Substrates, Wetting Angle Measurements

Surface free energy measurements were conducted on the TPU substrate before and after thermal treatment. Measurements were taken on the areas with printed graphene patterns to compare them with the substrate. Table 1 presents contact angles for diiodomethane and water, along with the calculated values of surface free energy and its components. The SFE was calculated using the Owens-Wendt method.[35] Figure 1 illustrates the contact angles observed on various surface films, pre- and post-thermal treatment, as well as on the deposited graphene layers.

Thermal treatment of TPU film resulted in a slight decrease in the water contact angle from 88.9° to 84.2°. Consecutively, the polar component of SFE increased from 1.9 to 4.6 mJ/m2. Substrate wettability is believed to be a major determinant of cell viability and surface cytocompatibility; hydrophobic substrates with high surface energies are considered to favour cell detachment.[16] Nascimento et al reported that for appropriate cell attachment and proliferation the ideal contact angle should be within the range 60°–70°.[54] The measured wetting angles have much higher values than suggested in the literature, which is probably due to the hydrophobic nature of graphene flakes. The decrease in the wetting angle after heating the TPU films may be related, among other things, to the removal of stresses in the material remaining after the manufacturing process. After heating, TPU films, through increasing the polar component of SFE, should exhibit higher adhesion of the printed ink. For this reason, previously heated substrates were used for further work.

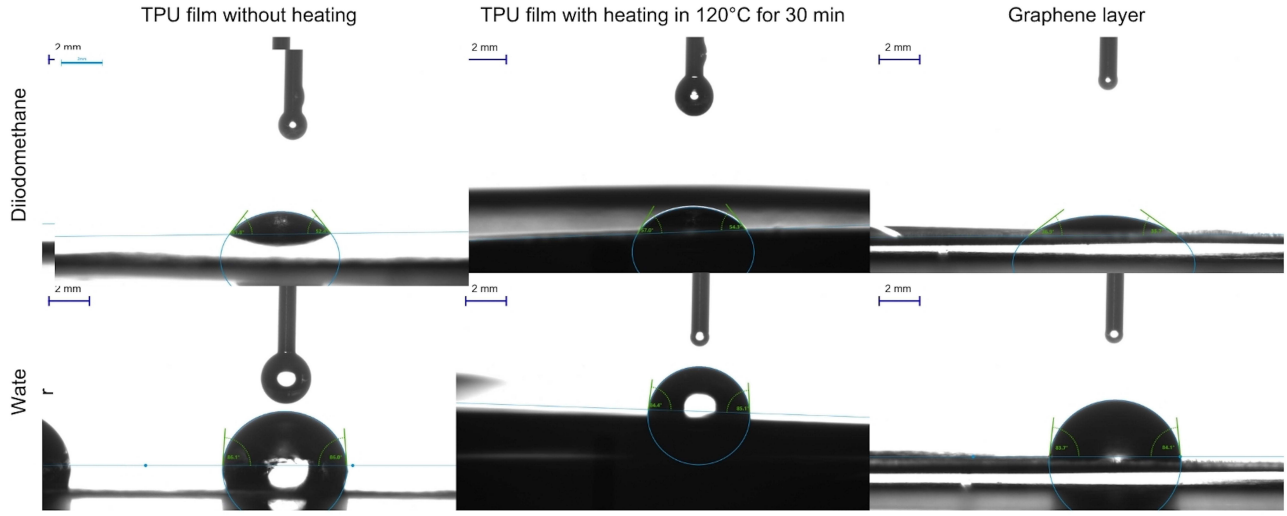

Figure 1 Measurement of wetting angles were conducted for TPU film without heating, TPU film heated for 30 minutes at 120 °C, Graphene layer. Each material was measured using diiodomethane and water.

The relation between SFE and their effect on cell adhesion remains not fully studied, with literature suggesting significant discrepancies on this topic. Hallab et al observed a proportion between surface energy and cell adhesion, indicating that materials with higher surface energy (as observed with metallic substrates) exhibit higher cell adhesion.[34,55] However, excessively high SFE inhibits cell adhesion, likely due to impaired adhesion of various proteins from the cell membrane to the substrate.[2] The printed graphene layers exhibited significantly higher SFE (42.6 mJ/m²) compared to TPU films (35.6 and 32.7 mJ/m² for TPU film before and after thermal treatment, respectively). However, the observed values are substantially lower than those reported in the literature as efficacious.[2,17,55] Nonetheless, when considered in conjunction with the engineered surface topography, a synergistic effect in cellular response can be postulated. This phenomenon warrants further investigation to elucidate the precise mechanisms underlying the potential synergistic effects and to quantify their impact on cellular adhesion, proliferation, and differentiation.

Substrate Prints and Characteristics

Micro and Macrogeometry of the Prints

Patterns were printed at intervals of 2 mm, 1 mm, and 0.5 mm. However, due to the spreading of ink on the substrates, the actual inter-print distances were reduced, as presented in Table 2. The average height and area of the prints, as measured by profilometry, are also provided in Table 4. Figures 2 and 3 present a comparative analysis of graphene prints on TPU substrates produced by IJP and AJP, captured at two distinct magnifications.

For a series of 20 prints (AJP and IJP each), the average height and cross-sectional area were measured. The mean print height of the AJP prints (7.71 ± 0.66 μm) exceeded that of the IJP prints (7.08 ± 0.42 μm). The mean height values are statistically different from each other at $p \leq 0.05$ ($p = 0.001$, $F = 12.45$), suggesting a statistically significant impact of the printing technique on printed line geometry. The average cross-sectional area followed the same trend: AJP lines (904.68 ± 44.63 μm²) were markedly narrower than their IJP counterparts (1054.4 ± 65.5 μm²). Normality of residuals was assessed with the Shapiro–Wilk test (AJP: $W = 0.83$, $p = 0.002$; IJP: $W = 0.94$, $p = 0.27$). One-way ANOVA is generally robust to moderate departures from normality with equal group sizes. Nevertheless, we verified the result with non-parametric Mann–Whitney *U*-test. One-way ANOVA confirmed that the difference is highly significant ($p < 0.001$, $F = 67.82$), a finding that remained significant when the data were re-analysed with the non-parametric Mann–Whitney *U*-test ($p < 0.001$). Thus, both height and cross-sectional area point to a clear influence of printing technique on the line geometry.

In the case of IJP substrates, a significant flow of ink can be observed, related to the high wettability of the substrate. Additionally, high-boiling-point solvents in the ink composition, while preventing cavitation bubbles in the print head, extend the evaporation time, causing further ink spreading on the substrate.[56–58] The morphology of IJP lines is influenced by multiple parameters, including ink composition, inter-drop distance and delay, temperature (ambient, substrate, and ink) and evaporation of solvent from individual droplets. IJP prints exhibit characteristic scalloping, potentially caused by excessive inter-drop distances.[59]

During printing, several undesirable phenomena can occur, including coffee ring formation and droplet path deviation in IJP, and overspray in AJP.[48,56,60,61] AJP prints exhibit greater surface roughness resulting from the deposition of significantly smaller ink droplets and additional solvent evaporation during ejection from the nozzle onto the substrate. In turn, in the case of IJP prints, the phenomenon of particle flocculation can occur. The inherent tendency of nanoparticles to agglomerate may lead to flocculation post-deposition, causing graphene particles to concentrate at the wet droplet's centre, leaving polymer at the printing interface.[62,63] This phenomenon may also result from the use of high-boiling-point solvents, which, during slow evaporation, lead to particle aggregation due to convective transport of graphene nanoplatelets towards the contact line.[64] In IJP, material is deposited as droplets, unlike AJP where the ink is almost completely

Table 4 Dimensions of Printed Lines and Grids/Meshes

	Average Height [μm]	Average Cross-Section Area [μm²]	Average Width [μm]
IJP	7.08±0.42	904.68 ± 45.79	108.25 ± 13.71
AJP	7.71 ± 0.66	1054.42 ± 114.86	90.35 ± 4.67

https://doi.org/10.2147/NSA.S530959

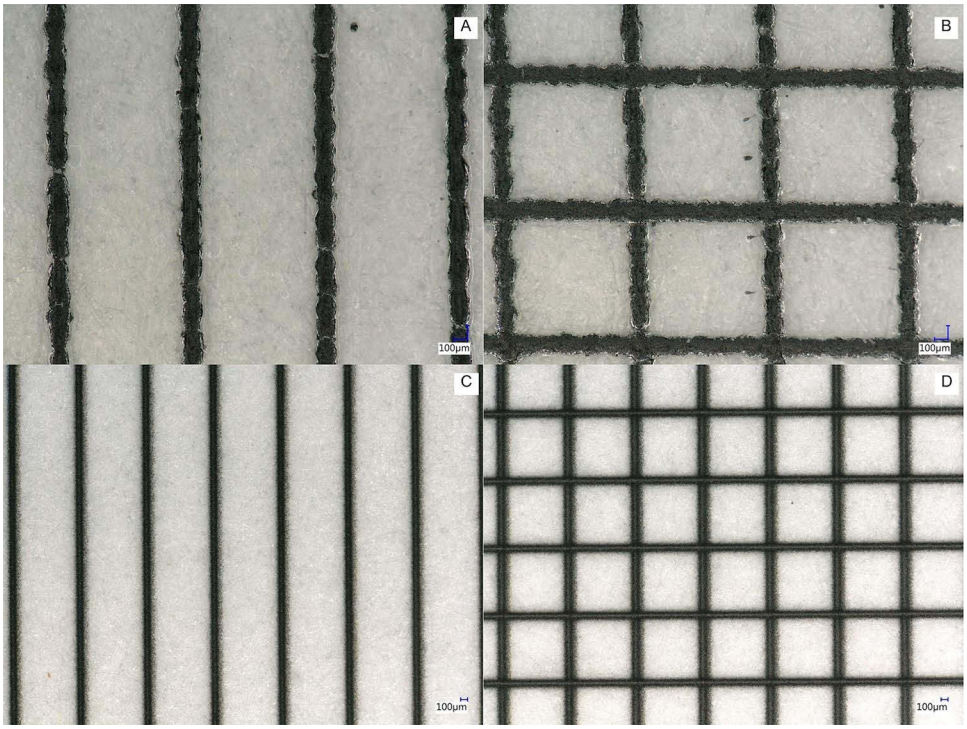

Figure 2 Line prints on TPU substrates printed with IJP (**A** and **B**) and AJP (**C** and **D**) Scale bar 100 µm.

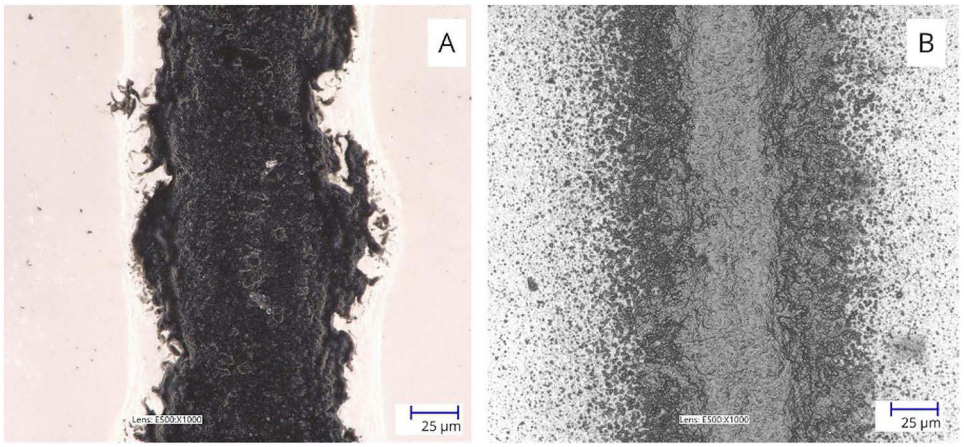

Figure 3 Detailed topographny of GNP Line prints on TPU substrates (**A**) Ink-jet printed line (**B**) Aerosol-jet printed line.

evaporated from the solvent mist.[65] Additionally, gravitational forces cause particles to settle towards the substrate during subsequent droplet deposition, resulting in polymer remaining on the printed pattern surface, as illustrated in Figure 3.

Particle behaviour in the printing process is governed by buoyancy, gravity, and drag forces, which influence dispersibility and sedimentation.[66] During droplet generation and descent, these forces affect the alignment of particles suspended within the picolitre volume of each droplet. Substrate contact further influences particle distribution, partly due to particle migration toward the droplet centre driven by surface tension gradients, resulting in the coffee ring effect.[64,67] Factors such as material surface tension, solvent evaporation rate, and ink composition (eg, surfactant inclusion) impact wet droplet behaviour on the substrate.[56,65]

This study focused on examining cell behaviour on different substrate geometries and determining which micro-printing technique is preferred by cells. While line geometry clearly affects the forces and pressures exerted by cells and

their ability to move and migrate, our primary objectives were to achieve print reproducibility, confirm prints cytocompatibility, and verify substrate preference of the cells.

To further determine the effect of the substrate material on the cells, Scanning Electron Microscopy (SEM) imaging was conducted to examine the microstructure of the prints. The results revealed clear differences in the printed paths (Figure 4). The AJP paths exhibited high porosity and surface roughness, attributed to the stacked structure of graphene nanoplatelets. In contrast, the IJP-produced paths display lower surface roughness with polymer-sealed pores. This distinction arises from the fundamental differences between the two printing techniques. In AJP, partially dried aerosol mist reaches the substrate, and a continuous stream of aerosol builds up a structure that becomes porous during the printing process. Conversely, in IJP larger ink droplets are deposited, coalescing into a continuous path on the substrate. This process results in the ink drying from the surface downward, creating a more uniform surface layer.

Elemental composition analysis was performed to compare the carbon and oxygen content of the samples. Figure 5 and Table 5 present the Energy-Dispersive X-ray Spectroscopy (EDS) results for IJP and AJP samples.

A notable difference in elemental composition was observed, with AJP tracks exhibiting higher carbon content. This phenomenon can be attributed to the distinct deposition mechanisms of the two printing methods. The material deposition process in AJP printing results in the predominance of the carbon phase on the surface of the printed pattern. In contrast, the nature of IJP leads to carbon material being encapsulated by polymer, resulting in a higher percentage of oxygen in the print composition. Furthermore, the observed differences may also be influenced by the spatial distribution of material within and on the surface of the printed path. This is particularly relevant considering the greater width of IJP-printed paths relative to AJP paths.

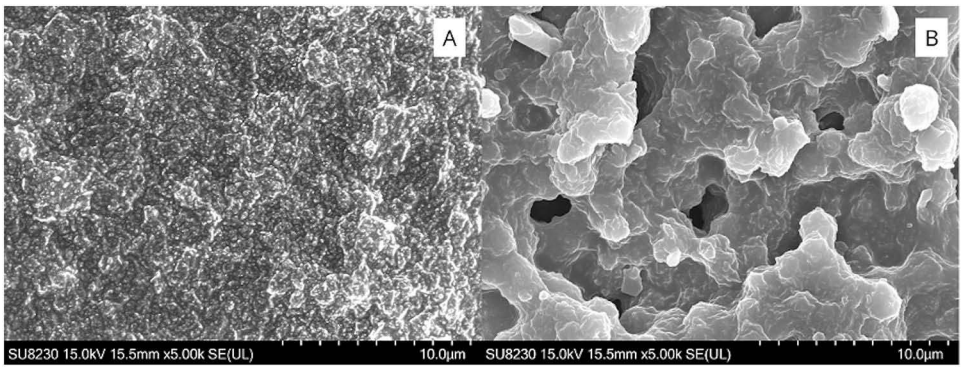

Figure 4 Scanning electron microscope images showing microgeometry of coatings: (**A**) Ink-jet printed line surface (**B**) aerosol jet printed line surface.

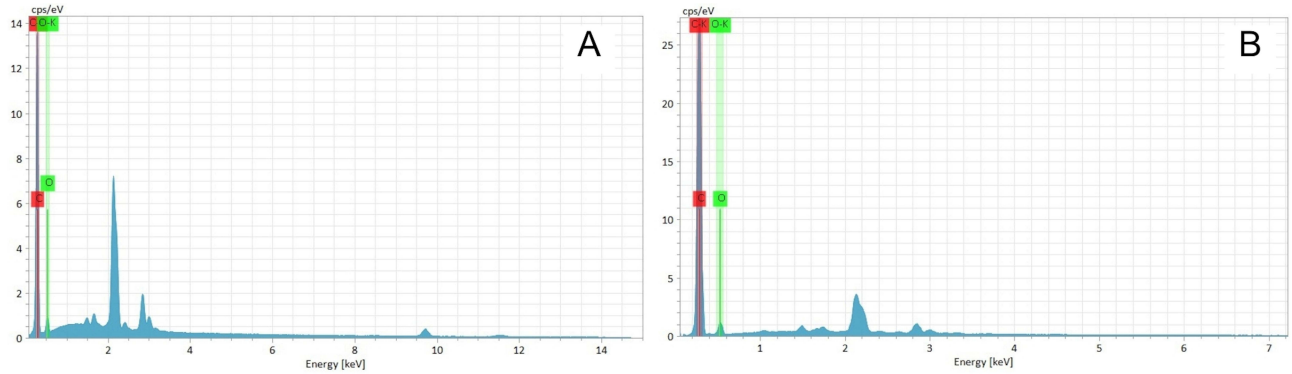

Figure 5 EDS spectroscopy results for (**A**) IJP and (**B**) AJP prints.

https://doi.org/10.2147/NSA.S530959

Table 5 EDS Spectroscopy Results – Oxygen and Carbon Content in AJP and IJP Prints

	Element	Atomic Number	Net Counts	Norm. Mass Concentration /%	Norm. Atomic Concentration /%	1σ Uncertainty/ mass%	1σ rel. Uncertainty /%
IJP	Carbon	6	104,178	81.71	85.61	1.27	1.56
	Oxygen	8	6102	18.29	14.39	0.47	2.58
AJP	Carbon	6	210,681	85.17	88.44	1.29	1.51
	Oxygen	8	8906	14.83	11.56	0.35	2.36

Profilometry Results

The topography of printed surfaces was assessed to evaluate the influence of surface patterning on cell growth and migration preferences. Each printed surface was examined in three distinct path sections using a contact profilometer. The measurement results are presented graphically, illustrating the cross-section of the path and the path roughness along the printing direction and providing insight into the homogeneity of print height. The profile characteristics are presented through multiple visualizations for both AJP and IJP: a 2D top-down graphical representation of the print (Figures 6a, 7a), a representative 3D optical profilometer image (Figures 6b, 7b) and roughness measurement in the X axis (Figures 6c, 7c) and cross-section profile in Y axis (Figures 6d, 7d).

Cross-sectional profiling revealed distinct differences in microgeometries between printing techniques. IJP produced consistent, smooth lines, while AJP generated paths with significant roughness and frayed outlines. These differences reflect varied ink behaviour associated with each deposition method. IJP utilizes droplets approximately 50 μm in diameter, facilitating the formation of a smooth, levelled layer before solvent evaporation creates a rigid printout. Conversely, AJP employs droplets 1–5 μm in diameter, leading to extensive solvent evaporation during droplet flight, mitigating the flooding effect on the substrate while resulting in a highly rough printout structure. Path heights for both techniques ranged from 10–15 μm.

The cross-sectional height profiles (Figures 6d, 7d) reveal that IJP achieved lower heights with wider prints, influenced by ink spread on the substrate, while AJP overprints produced higher, relatively narrower paths, disregarding the overspray area. The disparate printing processes of IJP and AJP resulted in markedly different surface morphologies. IJP produced relatively uniform surfaces with symmetrical paths, gradually increasing edge inclination angles, and lower roughness compared to AJP prints. Taller, more rough microprints arrays from AJP, due to increased surface area, might enhance protein absorption causing more extensive focal adhesion formation.[68] However, too high a roughness of the surface can hinder the migration of cells and their flattening on the surface, resulting in increased cell mortality.[69] Uniformity of IJP prints stems from a lower solvent evaporation rate than in AJP, where solvent evaporates during droplet flight. IJP's larger droplet volumes and lower evaporation rates allow prolonged substrate wetting, yielding more uniform paths.

Literature regarding the effect of surface roughness on cell adhesion remains, in some parts, contradictory.[2,55,70] Hallab et al found no statistically significant effect of roughness on cellular adhesion strength for high surface energy materials but observed significant differences for lower surface energy polymers.[55] Majhy et al demonstrated inhibition of cell growth on smooth surfaces. Conversely, Carpenter et al reported increased initial cell adhesion on altered topographies and culture surfaces due to enhanced protein adhesion.[2,34]

The distinct droplet sizes and solvent evaporation rates inherent to IJP and AJP not only determine the topography but also affect the reproducibility of cell responses. IJP's uniformity might be preferred for reproducibility of the studies, while AJP's variability could be useful for mimicking in vivo microenvironments where cells encounter diverse topographical cues. These findings suggest that factors beyond mere roughness affect cell behaviour, necessitating consideration of additional surface features and their variability in culture substrate design.

Resistivity Studies

To evaluate the potential use of printed substrates as conductive substrates for cellular electrostimulation we determine the printout resistivity. Two series of test lines were fabricated for IJP and AJP prints. Line length, average cross-

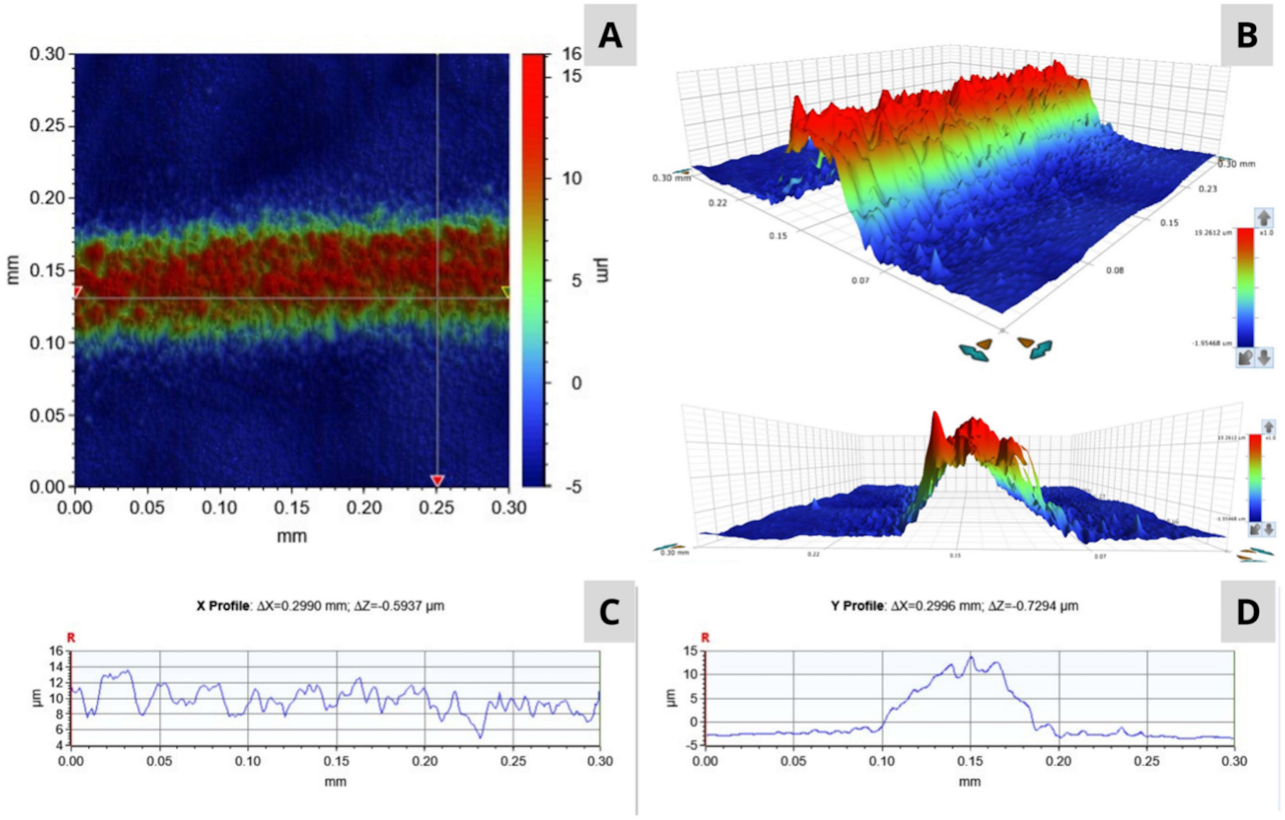

Figure 6 AJP profilometry results: (**A**) 2D top-down graphical representation of the printed line (**B**) 3D representation of the prints (**C**) Roughness measurement in X axis (**D**) Cross-section profile in Y axis.

sectional area, and resistance were measured to calculate the printout resistivity. The median resistivity of AJP lines ($2.8 \cdot 10^{-3}$ Ω m [IQR = $1.15 \cdot 10^{-3}$ Ω m]) exceeded that of IJP lines ($2.1 \cdot 10^{-3}$ Ω m [IQR = $0.65 \cdot 10^{-3}$ Ω m]). The Mann–Whitney test confirmed that this difference is statistically significant (U = 308, p = 0.004, r = 0.54). A robustness check using Welch's *t*-test on log-transformed values yielded an equivalent result (p = 0.009). Thus, the printing technique influences not only line geometry but also electrical resistivity.

The difference in resistivity results between these values can be attributed to the varied microgeometry of the printouts obtained with each fabrication method. The distribution of the functional phase within the cross-section of IJP and AJP prints exhibits distinct differences, as previously discussed. Research has demonstrated that in IJP prints, graphene flakes undergo sedimentation and preferentially deposit near the substrate. This results in overlapping flakes that are isolated from the carrier polymer matrix, forming a more conductive pathway compared to AJP prints. Conversely, in AJP prints, the presence of graphene flakes on the print surface has been experimentally verified. These observations suggest that the graphene functional phase in AJP prints is more uniformly distributed throughout the polymer carrier, which may restrict direct contact and overlapping of graphene flakes.

Raman Spectroscopy Studies

The chemical structure of each pattern was further characterized using Raman spectroscopy. The Raman profiles of the pattern inks exhibited distinct differences between AJP and IJP samples (Figure 8).

In AJP patterns, the expected D and G peaks, resulting from primary in-plane vibrational modes, are observed at 1345 and 1584 cm^{-1}, respectively. The D peak, related to the breathing modes of six-atom rings, typically correlates with structural defects. The G peak, associated with graphitic carbon, arises from bond stretching of sp^2 pairs in both carbon

https://doi.org/10.2147/NSA.S530959

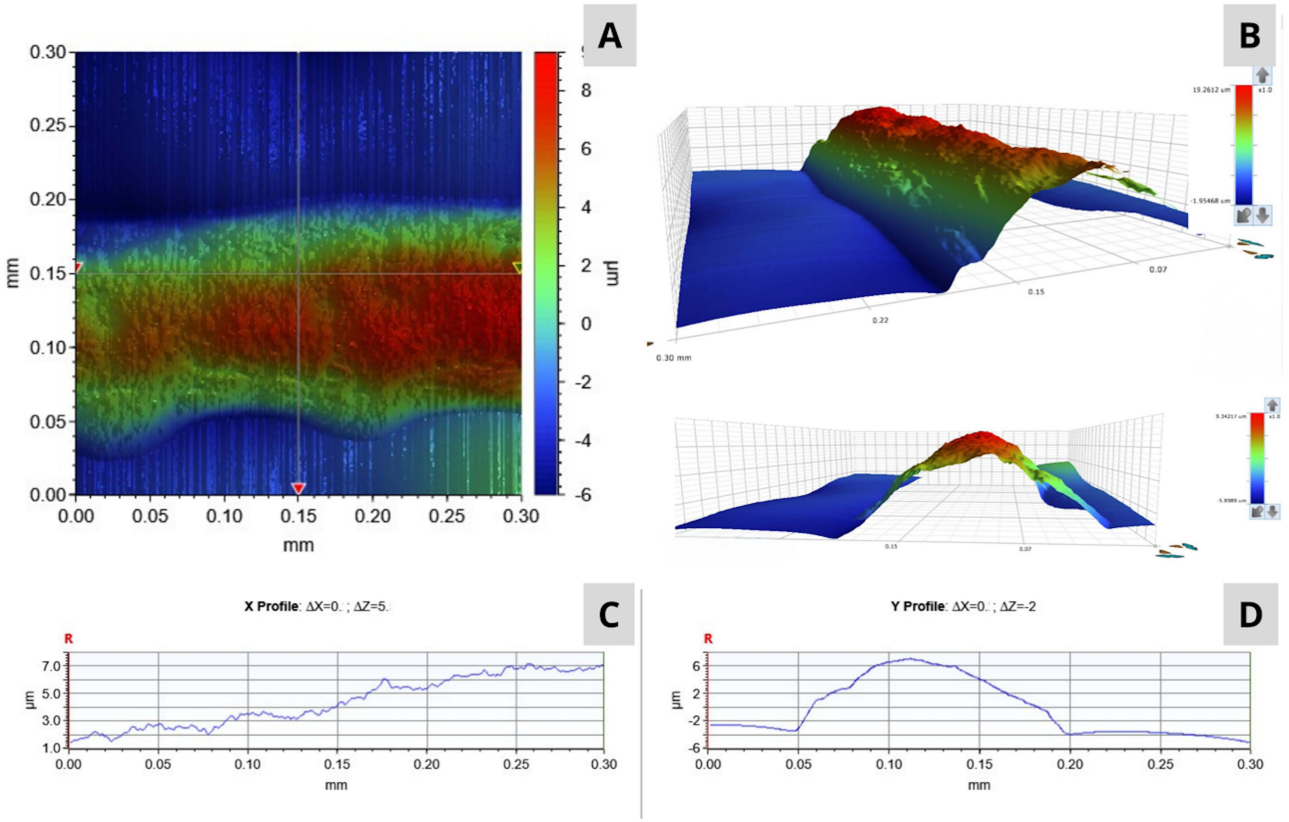

Figure 7 IJP profilometry results: (**A**) 2D top-down graphical representation of the printed line (**B**) 3D representation of the prints (**C**) Roughness measurement in X axis (**D**) Cross-section profile in Y axis.

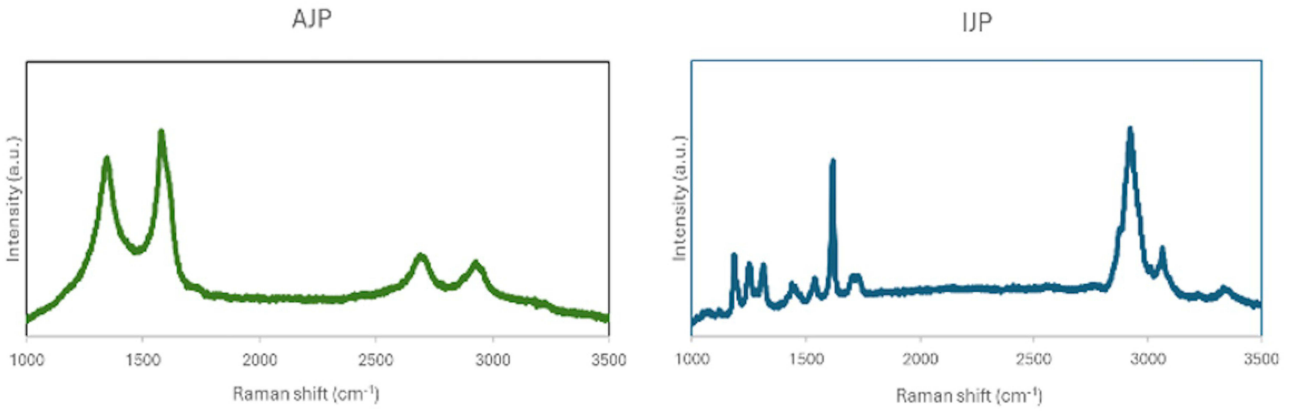

Figure 8 Raman spectroscopy results for AJP and IJP prints.

rings and chains. Additionally, the 2D peak is detected at 2682 cm^{-1}, attributable to the second-order overtone of the D vibration. A broad D + D' band is also observed at 2936 cm^{-1}.[71,72] In the IJP pattern, the observed peaks are consistent with TPU vibrations.[73] Specifically:

- The peak at 2926 cm^{-1} is attributed to the stretching vibrations of $–CH_2$
- Peaks at 1727 cm^{-1} and 1701 cm^{-1} are due to carbonyl stretching vibrations
- A strong peak at 1615 cm^{-1} can be assigned to the symmetric stretching of aromatic C=C vibrations

- The peak at 1537 cm^{-1} is due to C=C stretching of urethane amide
- The peak at 1437 cm^{-1} is assigned to the bending vibrations of $–CH_2$

The differences in Raman spectra between AJP and IJP can be attributed to variations in layer porosity, roughness, and the interaction of graphene nanoplatelets (GNP) with the polymer matrix. The AJP method preserves the structural characteristics of graphene, leading to distinct Raman peaks. In contrast, the IJP method creates a more uniform polymer-rich surface, which obscures the graphene signals. This observation is corroborated by the micro and macrotopography images (Figures 3 and 4).

MTT Assay

MTT assay revealed that all tested materials, including uncoated TPU film and all variants of materials coated with graphene patterns and layers, have been proven non-cytotoxic, as their corresponding cell viabilities were above 70% as shown in Figure 9. It was determined that extracts obtained with 72 hours of extraction, which is a required extraction time for biomaterials designed for implantation, showed no evidence of toxicity, regardless of the graphene content and surface topography.

The MTT assay results clearly demonstrate that both the uncoated TPU substrate and all graphene-coated substrates are generally non-cytotoxic to L929 fibroblasts. Similar findings have been reported in the literature, further confirming that graphene coatings exhibit favourable cytocompatibility.[74] Based on these results, it can be concluded that the printing method used for graphene deposition does not adversely influence cell viability. Although previous studies have reported that cytotoxicity can vary depending on graphene concentration, surface chemistry, and morphological form, our findings suggest that even relatively high graphene content remains safe for L929 fibroblasts under the conditions tested.[75] Nevertheless, overall biocompatibility of the substrates should be further evaluated through complementary assays, including longer-term culture studies and assessments of potential inflammatory responses, to ensure their suitability for biomedical applications.

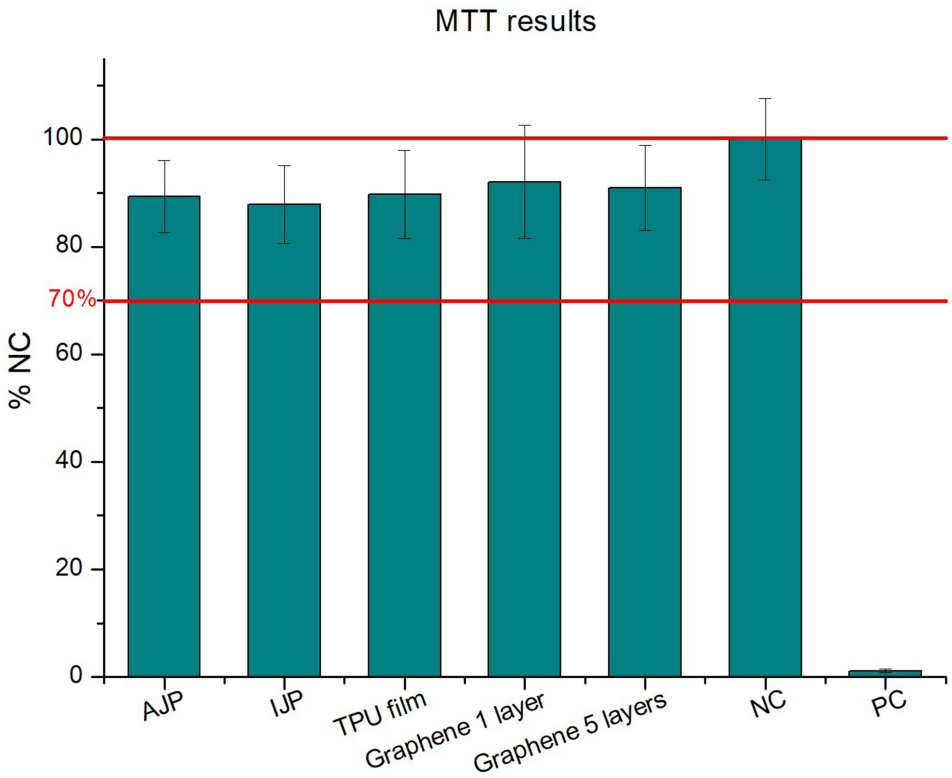

Figure 9 Cell viability determined with MTT assay for cells cultured on AJP and IJP prints, TPU foil without patterning, TPU foil with 1 layer of graphene layer, TPU foil with 5 layers of graphene, negative control (NC) and positive control (PC).

https://doi.org/10.2147/NSA.S530959

Effect of Surface Patterning and Physicochemical Properties on Cell Growth and Proliferation

Figure 10 presents a comparative analysis of cell images obtained using confocal microscopy, after staining with AlexaFluor 488 for actin cytoskeleton visualization at 24 and 72 hours of culture. Control cultures and more detailed photographs can be found in the Supporting Information (Figures 6–8). In these images, the black bars represent the graphene prints on which the cells are adhered. It is important to note that the substrates were not pre-treated with any adhesion-promoting coatings or hydrophobic coatings to repel cells from the substrate (such as laminin or prior immersion in culture medium).

Morphological changes of cells were observed on both graphene and control substrates. After 24 hours of incubation, cells initially exhibiting a rounded morphology transitioned into a spindle-shaped form, characteristic for fibroblasts. The control culture on TPU substrates exhibited no signs of cytotoxicity, with cells evenly populating the entire substrate. At both time points, graphene patterned substrates with denser printing, such as grids and 0.5 mm lines, demonstrated larger areas of cell coverage and higher cell density. On lines spaced at greater distances – 2 mm and 1 mm, L929 fibroblasts grew relatively evenly; however, numerous areas of cell migration were observed at the print edges, particularly in case of IJP patterns.

As was proven by imaging, profilometry and spectroscopy, the AJP printed patterns are distinguished by the entirety of the surface being filled with graphene flakes, allowing cells to be in direct contact with GNP. In contrast, IJP printing results in a higher presence of TPU on the surface, with graphene particles mostly deposited beneath, which may explain the superior results of cell growth and attachment observed for AJP printing. The development of highly conductive yet biocompatible coatings incorporating nanomaterials presents new opportunities in tissue engineering. Conventional two-dimensional (2D) substrates, such as glass or tissue culture plastic, fail to replicate the complicated architecture of native tissue and are therefore suboptimal for studies aiming to reproduce complex cellular structures and functions.[46,76] Substrate properties play a decisive role in modulating cellular responses. Feng Lin et al demonstrated that the stiffness of graphene substrates regulates single-layer graphene (SLG)-induced fibroblast adhesion and proliferation.[77] Similarly, Sachin Kumar reported that the underlying substrate exerts a significant influence on graphene-mediated cellular behavior.[78] These findings underscore the importance of substrate mechanics in the performance of graphene-based materials and highlight the need for further systematic investigation in this domain. Carbon-based nanomaterials, due to their nanoscale dimensions, can replicate structural characteristics of the extracellular matrix (ECM), providing a biomimetic and electrically conductive environment that supports cellular growth and differentiation. Graphene-based substrates possess in-plane bonding characteristics that promote protein adsorption—an essential step in cellular function—and have been shown to enhance neurite outgrowth and cell proliferation compared with conventional glass substrates.[79–82] Their mechanical flexibility further enables them to conform to the geometries of injured tissues, facilitating targeted stimulation of damaged sites.[22] These properties confer distinct advantages over widely used biomaterials such as glass, polystyrene, hydrogels, and collagen.[20,79] Graphene substrates fabricated via additive manufacturing exhibit both high flexibility and substantial mechanical strength, surpassing natural biopolymers and hydrogel-based constructs for a range of biomedical applications.[83]

Cell adhesion to such substrates is mediated by short-range physicochemical interactions, including hydrogen bonding, van der Waals forces, Coulombic interactions, steric forces, and strong associations with carboxyl functional groups (–COOH). This phenomenon is regulated by cell-substrate interactions controlled by integrins in the cell lamina and surface free energy components. An increase in SFE—along with a rise in hydroxyl and carboxyl group density—promotes hydrogen bond formation with cell surface lipids and ions. This, in turn, enhances cell adhesion, proliferation, and growth.[6] As a result, our graphene substrates, with their tuneable mechanical properties, hold considerable promise for the regulation of cellular functions.

In our study, L929 fibroblasts exhibited preferential alignment and migration along graphene nanoplatelet (GNP) lines and grid patterns with narrow 0.5 mm gap distances. Cells cultured on GNP grid patterns—particularly those with 1 mm and 2 mm Aerosol Jet Printing (AJP) grids—displayed distinct orientation and a marked tendency to migrate toward printed regions compared with non-GNP-coated thermoplastic polyurethane (TPU) areas. Notably, cells overlapped and

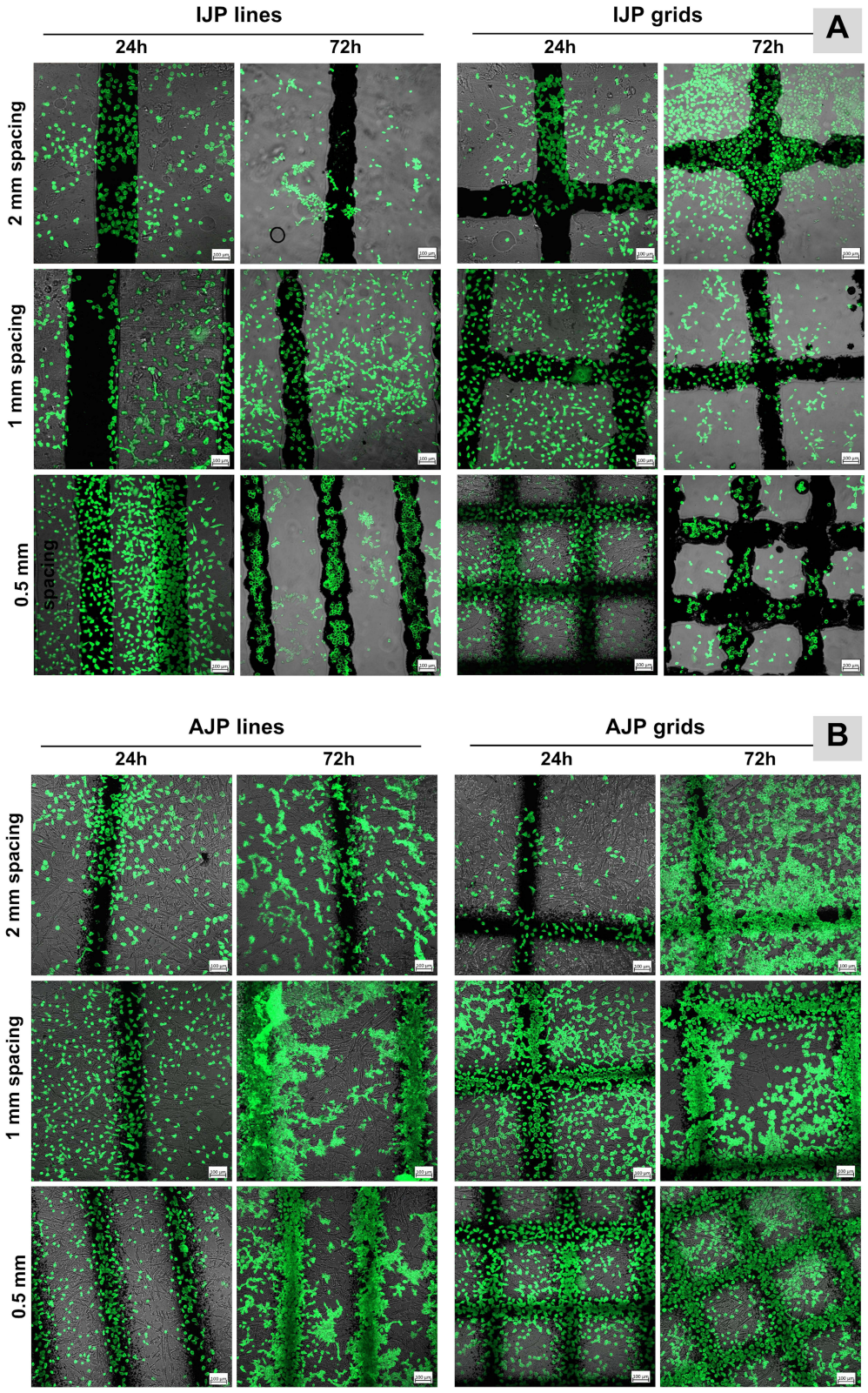

Figure 10 Morphological staining of L929 cells on (**A**) ink-jet patterned substrates and (**B**) aerosol-jet patterned substrates in two timepoints 24h and 72h, for lines and grids in two spacings: 2mm, 1mm and 0.5 mm.

https://doi.org/10.2147/NSA.S530959

aligned along the central axis of the printed lines, occupying most of the graphene-coated regions, especially at points corresponding to the highest profile height above the substrate. In addition to SFE, substrate roughness and geometric features were found to significantly influence cell–substrate interactions. These observations highlight the limitations of conventional flat culture platforms and reinforce the role of engineered topographical features in directing cell behaviour. Despite exhibiting a relatively high wetting angle of 87.3° ± 6.5, the graphene patterns promoted robust cell adhesion and proliferation. Based on the obtained results, it can be inferred that potential biocompatibility should not be considered solely based on the wetting angle value, as the phenomenon is ultimately influenced by multiple substrate properties, such as surface energy and material topography. Instead, cellular responses are determined by a combination of physicochemical factors (surface energy, functional group chemistry) and physical parameters (roughness, topography).

While there are studies investigating printed graphene-based layers in tissue engineering, there is no literature exploring the use of microprinted AJP layers to control cell behaviour via substrate topography. Our results further indicate that topographical variations arising from different printing modalities influence cellular responses. AJP-printed graphene patterns exhibited a gradual increase in profile height, creating elevated "platform-like" structures that facilitated directed cell migration. The wider printed paths and discrete ink droplets may have served as anchoring points, enabling cell attachment and upward migration. By contrast, inkjet-printed (IJP) paths were smoother, owing to a higher polymer concentration near the surface, which may have impeded adhesion and migration. These findings confirm that substrate geometry serves as a potent topographical cue guiding cell localization. The high precision and scalability of AJP technology make it particularly well suited for producing biologically relevant microstructures, such as collagen architectures for bone tissue engineering or protein/enzyme arrays.[24,41,49]

Although our findings demonstrate that microprinted GNP patterns are not cytotoxic, can effectively enhance cellular alignment and migration, several limitations must be acknowledged.

Although they outperform conventional flat culture platforms in guiding cell behaviour, they remain an approximation of in vivo conditions. While our prints have demonstrated favourable cytocompability in vitro, their potential cytotoxicity remains a critical consideration for future in vivo applications. The biological response to GNPs can vary significantly depending on particle size, layer number, surface chemistry, oxidation state, and the presence of residual processing additives. Future work should address challenges such as optimizing ink formulations for minimal interference with biological processes, enhancement adhesion to various substrates and conductivity for future research including electrostimulation.[21,82]

Our findings indicate that graphene-based microprinted substrates hold considerable promise for tissue regeneration strategies. Future work should prioritize quantitative correlation between Ra/Rq values and cell behavior for providing deeper mechanistic insight info cell migration, elucidating the synergistic effects of combined topographical and electrical cues on stem cell alignment, investigating the influence of these biophysical stimuli on lineage-specific stem cell differentiation. Such studies will be critical in unlocking the full potential of graphene microprinting to advance regenerative medicine and improve clinical outcomes.

Conclusion

In this study, we successfully utilized graphene nanoplatelet-based ink to create specialized substrates that effectively promote cell proliferation. The primary objective was to investigate the behavioral preferences of L929 fibroblast cells cultured on graphene substrates prepared using two microprinting techniques — inkjet printing and aerosol jet printing — using the same composite material to fabricate precisely defined patterns. The study sought to determine whether there is a significant difference in cellular preference for the topography of the printed surface resulting from the use of these distinct printing techniques. We designed two types of patterns (lines and grids) with three different distances (2, 1, and 0.5 mm) and comprehensively characterized them in terms of micro- and macro-morphology, Raman spectroscopy, substrate wettability, and surface free energy, followed by their effects on L929 cells behaviour.

Our findings revealed that the patterned graphene substrates exhibited biocompatibility, showing no cytotoxicity towards L929 cells and positively influenced cell proliferation. Importantly, we observed a clear cellular preference for the graphene patterns, cells adhering and proliferating more effectively on these surfaces. This behaviour can be attributed to the unique physicochemical properties of graphene, including its high surface area, favourable surface energy, and ability to provide nanoscale topographical cues that guide cellular responses. Among the two printing

techniques evaluated, patterns produced using aerosol jet printing were particularly favourable. The enhanced cellular response for AJP is most likely due to a higher concentration of exposed graphene nanoplatelets on the surface and a more advantageous cross-sectional roughness profile, which together facilitated improved initial cell attachment, spreading, and subsequent proliferation.

These results underscore the potential of microprinted graphene paths, printed using microprinting techniques as advanced platforms for guiding cell behaviour. The demonstrated ability to modulate cell adhesion, spreading, and proliferation through precise surface patterning highlights the significant promise of these materials in a variety of biomedical applications. In particular, the developed graphene-based substrates have strong potential to serve as functional scaffolds for tissue regeneration, where spatial organization and controlled cellular responses are critical for successful integration and tissue repair. Moreover, the capacity to fine-tune surface architecture using different microprinting techniques opens new opportunities for creating customizable, patient-specific implants and advanced biointerfaces. Overall, this approach represents a substantial advancement in tissue engineering and regenerative medicine, providing innovative strategies for the design of next-generation biomaterials that promote healing, improve tissue integration and support long-term clinical success.

Data Sharing Statement

The data that support the findings of this study are available from the corresponding author upon reasonable request.

Author Contributions

All authors made a significant contribution to the work reported, whether that is in the conception, study design, execution, acquisition of data, analysis and interpretation, or in all these areas; took part in drafting, revising or critically reviewing the article; gave final approval of the version to be published; have agreed on the journal to which the article has been submitted; and agree to be accountable for all aspects of the work.

Funding

Research was funded by the Warsaw University of Technology within the Excellence Initiative: Research University (IDUB) program (Grant YOUNG PW II) 504/04496/1101/45.180001 and the European Union's Horizon 2020 Research and Innovation Program under Grant Agreement No. 101008701 (EMERGE, H2020-INFRAIA-2020-1). The research was also conducted with the Associate Laboratory Institute of Nanostructures, Nanomodelling and Nanofabrication-i3N (through FCT – Portuguese Foundation for Science and Technology, through projects LA/P/0037/2020, UIDP/50025/2020 and UIDB/50025/2020) and M.C.C. acknowledges FCT for the researcher contract (2021.03255.CEECIND).

Disclosure

The authors report no conflicts of interest in this work.

References

1. Waiwijit U, Maturos T, Pakapongpan S, Phokharatkul D, Wisitsoraat A, Tuantranont A. Highly cytocompatible and flexible three-dimensional graphene/polydimethylsiloxane composite for culture and electrochemical detection of L929 fibroblast cells. *J Biomater Appl*. 2016;31(2):230–240. doi:10.1177/0885328216656477
2. Majhy B, Priyadarshini P, Sen AK. Effect of surface energy and roughness on cell adhesion and growth – facile surface modification for enhanced cell culture. *RSC Adv*. 2021;11(25):15467–15476. doi:10.1039/D1RA02402G
3. Kyu Lee S, Kim H, Sup Shim B, Info A. Graphene: an emerging material for biological tissue engineering. *Carbon Lett*. 2013;14(2):63–75. doi:10.5714/CL.2013.14.2.063
4. Kumar R, Rauti R, Scaini D, et al. Graphene-based nanomaterials for neuroengineering: recent advances and future prospective. *Adv Funct Mater*. 2021;31(46):2104887. doi:10.1002/ADFM.202104887
5. Park J, Kim YS, Ryu S, et al. Graphene potentiates the myocardial repair efficacy of mesenchymal stem cells by stimulating the expression of angiogenic growth factors and gap junction protein. *Adv Funct Mater*. 2015;25(17):2590–2600. doi:10.1002/ADFM.201500365
6. Vlăsceanu GM, Iovu H, Ioniță M. Graphene inks for the 3D printing of cell culture scaffolds and related molecular arrays. *Compos B Eng*. 2019;162:712–723. doi:10.1016/J.COMPOSITESB.2019.01.010
7. Adamowicz J, Pasternak I, Kloskowski T, et al. Development of a conductive biocomposite combining graphene and amniotic membrane for replacement of the neuronal network of tissue-engineered urinary bladder. *Sci Rep*. 2020;10(1):1–15. doi:10.1038/s41598-020-62197-3
8. Stankovich S, Dikin DA, Dommett GHB, et al. Graphene-based composite materials. *Nature*. 2006;442(7100):282–286. doi:10.1038/nature04969

9. Ku SH, Lee M, Park CB. Carbon-based nanomaterials for tissue engineering. *Adv Healthc Mater*. 2013;2(2):244–260. doi:10.1002/ADHM.201200307
10. Bai RG, Muthoosamy K, Manickam S, Hilal-Alnaqbi A. Graphene-based 3D scaffolds in tissue engineering: fabrication, applications, and future scope in liver tissue engineering. *Int J Nanomed*. 2019;14:5753–5783. doi:10.2147/IJN.S192779
11. Fan H, Wang L, Zhao K, et al. Fabrication, mechanical properties, and biocompatibility of graphene-reinforced chitosan composites. *Biomacromolecules*. 2010;11(9):2345–2351. doi:10.1021/BM100470Q/ASSET/IMAGES/MEDIUM/BM-2010-00470Q_0001.GIF
12. Galvagno E, Tartaglia E, Stratigaki M, et al. Present status and perspectives of graphene and graphene-related materials in cultural heritage. *Adv Funct Mater*. 2024;34(13):2313043. doi:10.1002/ADFM.202313043
13. Sahni D, Jea A, Mata JA, et al. Biocompatibility of pristine graphene for neuronal interface: laboratory investigation. *J Neurosurg Pediatr*. 2013;11(5):575–583. doi:10.3171/2013.1.PEDS12374
14. Wang M, Mi G, Shi D, Bassous N, Hickey D, Webster TJ. Nanotechnology and nanomaterials for improving neural interfaces. *Adv Funct Mater*. 2018;28(12):1–28. doi:10.1002/adfm.201700905
15. Krukiewicz K, Janas D, Vallejo-Giraldo C, Biggs MJP. Self-supporting carbon nanotube films as flexible neural interfaces. *Electrochim Acta*. 2019;295:253–261. doi:10.1016/j.electacta.2018.10.157
16. Sherrell PC, Thompson BC, Wassei JK, et al. Maintaining cytocompatibility of biopolymers through a graphene layer for electrical stimulation of nerve cells. *Adv Funct Mater*. 2014;24(6):769–776. doi:10.1002/ADFM.201301760
17. Park R, Kang MS, Heo G, Shin YC, Han DW, Hong SW. Regulated behavior in living cells with highly aligned configurations on nanowrinkled graphene oxide substrates: deep learning based on interplay of cellular contact guidance. *ACS Nano*. 2024;18(2):1325–1344. doi:10.1021/ACSNANO.2C09815/SUPPL_FILE/NN2C09815_SI_009.MP4
18. Kim TH, Shah S, Yang L, et al. Controlling differentiation of adipose-derived stem cells using combinatorial graphene hybrid-pattern arrays. *ACS Nano*. 2015;9(4):3780–3790. doi:10.1021/nn5066028
19. Chen GY, Pang DWP, Hwang SM, Tuan HY, Hu YC. A graphene-based platform for induced pluripotent stem cells culture and differentiation. *Biomaterials*. 2012;33(2):418–427. doi:10.1016/J.BIOMATERIALS.2011.09.071
20. Phan LMT, Tat V, Hoang TX, Cho S. Graphene integrated hydrogels based biomaterials in photothermal biomedicine. *Nanomaterials*. 2021;11(4):906. doi:10.3390/NANO11040906
21. Nicoletti NF, Marinowic DR, Perondi D, et al. Non-cytotoxic graphene nanoplatelets upregulate cell proliferation and self-renewal genes of mesenchymal stem cells. *Int J Mol Sci*. 2024;25(18):9817. doi:10.3390/IJMS25189817
22. Das JM, Upadhyay J, Monaghan MG, Borah R. Impact of the reduction time-dependent electrical conductivity of graphene nanoplatelet-coated aligned bombyx mori silk scaffolds on electrically stimulated axonal growth. *ACS Appl Bio Mater*. 2024;7(4):2389–2401. doi:10.1021/ACSABM.4C00052/ASSET/IMAGES/LARGE/MT4C00052_0005.JPEG
23. Ławkowska K, Pokrywczyńska M, Koper K, Kluth LA, Drewa T, Adamowicz J. Application of graphene in tissue engineering of the nervous system. *Int J Mol Sci*. 2021;23(1):33. doi:10.3390/IJMS23010033
24. Kanayama I, Miyaji H, Takita H, et al. Comparative study of bioactivity of collagen scaffolds coated with graphene oxide and reduced graphene oxide. *Int J Nanomed*. 2014;9(1):3363–3373. doi:10.2147/IJN.S62342
25. Sevimli G, Kus E, Baran G, Marashian M, Tabatabaei N, Mustafaoglu N. Graphene nanoplatelets enhance neuronal differentiation of human bone marrow mesenchymal stem cells. *Biol Res*. 2025;58(1):1–14. doi:10.1186/S40659-025-00616-3
26. Poorsargol M, Alimohammadian M, Sohrabi B, Dehestani M. Dispersion of graphene using surfactant mixtures: experimental and molecular dynamics simulation studies. *Appl Surf Sci*. 2019;464:440–450. doi:10.1016/j.apsusc.2018.09.042
27. Dybowska-Sarapuk Ł. Development of the production process of biocompatible, conductive graphene ink. 2019.
28. Dybowska-Sarapuk L, Sosnowicz W, Krzeminski J, et al. Printed graphene layer as a base for cell electrostimulation—preliminary results. *Int J Mol Sci*. 2020;21(21):7865. doi:10.3390/IJMS21217865
29. Dybowska-Sarapuk Ł, Szałapak J, Wróblewski G, Wyżkiewicz I, Słoma M, Jakubowska M. Rheology of inks for various techniques of printed electronics. *Adv Intellig Syste Comput*. 2016;393:447–451. doi:10.1007/978-3-319-23923-1_65
30. Dybowska-Sarapuk Ł, Sosnowicz W, Grzeczkowicz A, Krzemiński J, Jakubowska M. Ultrasonication effects on graphene composites in neural cell cultures. *Front Mol Neurosci*. 2022;15. doi:10.3389/fnmol.2022.992494
31. Wang S, Zhang Y, Abidi N, Cabrales L. Wettability and surface free energy of graphene films. *Langmuir*. 2009;25(18):11078–11081. doi:10.1021/LA901402F/SUPPL_FILE/LA901402F_SI_001.XLS
32. Wysotzki P, Sancho A, Gimsa J, Groll J. A comparative analysis of detachment forces and energies in initial and mature cell-material interaction. *Colloids Surf B Biointerfaces*. 2020;190:110894. doi:10.1016/J.COLSURFB.2020.110894
33. Okamura Y, Tagawa M, Gotoh K, Sunaga M, Tagawa T. Influence of drawing and heat treatment on surface free energies of polyethylene terephthalate fibers. *Colloid Polym Sci*. 1996;274(7):628–633. doi:10.1007/BF00653059/METRICS
34. Carpenter J, Khang D, Webster TJ. Nanometer polymer surface features: the influence on surface energy, protein adsorption and endothelial cell adhesion. *Nanotechnology*. 2008;19(50):505103. doi:10.1088/0957-4484/19/50/505103
35. Owens DK, Wendt RC. Estimation of the surface free energy of polymers. *J Appl Polym Sci*. 1969;13(8):1741–1747. doi:10.1002/APP.1969.070130815
36. Trzaskowska P, Rybak E, Jablonska - Lawniczak K, et al. The potential of electropolymerized crosslinked PEGDMA coating on steel for further functionalization: surface parameters and HMEC-1 cells attachment correlations. *Appl Surf Sci*. 2023;635:157761. doi:10.1016/j.apsusc.2023.157761
37. Smith AST, Choi E, Gray K, et al. NanoMEA: a tool for high-throughput, electrophysiological phenotyping of patterned excitable cells. *Nano Lett*. 2020;20(3):1561–1570. doi:10.1021/ACS.NANOLETT.9B04152/SUPPL_FILE/NL9B04152_SI_007.MP4
38. Gonçalves G, Borme J, Bdkin I, et al. Reductive nanometric patterning of graphene oxide paper using electron beam lithography. *Carbon NY*. 2018;129:63–75. doi:10.1016/J.CARBON.2017.11.067
39. Balikov DA, Fang B, Chun YW, et al. Directing lineage specification of human mesenchymal stem cells by decoupling electrical stimulation and physical patterning on unmodified graphene. *Nanoscale*. 2016;8(28):13730–13739. doi:10.1039/c6nr04400j
40. Phuah EWC, Hart WL, Sumer H, Stoddart PR. Patterning of biomaterials by aerosol jet printing: a parametric study. *Bioprinting*. 2020;18:e00081. doi:10.1016/J.BPRINT.2020.E00081

41. Tonello S, Bianchetti A, Braga S, et al. Impedance-based monitoring of mesenchymal stromal cell three-dimensional proliferation using aerosol jet printed sensors: a tissue engineering application. *Materials*. 2020;13(10):2231. doi:10.3390/MA13102231
42. Das SR, Uz M, Ding S, et al. Electrical differentiation of mesenchymal stem cells into schwann-cell-like phenotypes using inkjet-printed graphene circuits. *Adv Healthc Mater*. 2017;6(7). doi:10.1002/ADHM.201601087
43. Li J, Ye F, Vaziri S, Muhammed M, Lemme MC, Östling M. Efficient inkjet printing of graphene. *Adv Mater*. 2013;25(29):3985–3992. doi:10.1002/ADMA.201300361
44. Nayak L, Mohanty S, Nayak SK, Ramadoss A. A review on inkjet printing of nanoparticle inks for flexible electronics. *J Mater Chem C Mater*. 2019;7(29):8771–8795. doi:10.1039/C9TC01630A
45. Wilkinson NJ, Smith MAA, Kay RW, Harris RA. A review of aerosol jet printing—a non-traditional hybrid process for micro-manufacturing. *Int J Adv Manuf Technol*. 2019;105(11):4599–4619. doi:10.1007/S00170-019-03438-2/METRICS
46. Capel AJ, Smith MAA, Taccola S, et al. Digitally driven aerosol jet printing to enable customisable neuronal guidance. *Front Cell Dev Biol*. 2021;9:722294. doi:10.3389/FCELL.2021.722294/BIBTEX
47. Boland T, Xu T, Damon B, Cui X. Application of inkjet printing to tissue engineering. *Biotechnol J*. 2006;1(9):910–917. doi:10.1002/BIOT.200600081
48. Saunders RE, Derby B, Zhang J, Chen Y, Feng Y, Su Z. Inkjet printing biomaterials for tissue engineering: bioprinting. *J Human Genetics*. 2014;59(8):430–448. doi:10.1179/1743280414Y.0000000040
49. Degryse O, Bloemen V, Ferraris E. Collagen composite inks for aerosol Jet® printing in bone tissue engineering applications. *Procedia CIRP*. 2022;110(C):180–185. doi:10.1016/J.PROCIR.2022.06.033
50. Seiti M, Ginestra P, Ferraro RM, Ceretti E, Ferraris E. Nebulized jet-based printing of bio-electrical scaffolds for neural tissue engineering: a feasibility study. *Biofabrication*. 2020;12(2):025024. doi:10.1088/1758-5090/AB71E0
51. Niaraki A, Abbasi Shirsavar M, Aykar SS, Taghavimehr M, Montazami R, Hashemi NN. Minute-sensitive real-time monitoring of neural cells through printed graphene microelectrodes. *Biosens Bioelectron*. 2022;210:114284. doi:10.1016/J.BIOS.2022.114284
52. Zhu Y, Murali S, Cai W, et al. Graphene and graphene oxide: synthesis, properties, and applications. *Adv Mater*. 2010;22(35):3906–3924. doi:10.1002/adma.201001068
53. Lee WC, Lim CHYX, Shi H, et al. Origin of enhanced stem cell growth and differentiation on graphene and graphene oxide. *ACS Nano*. 2011;5(9):7334–7341. doi:10.1021/nn202190c
54. Do Nascimento RM, Sarig U, da Cruz NC, et al. Optimized-surface wettability: a new experimental 3D modeling approach predicting favorable biomaterial–cell interactions. *Adv Theory Simul*. 2019;2(7):1900079. doi:10.1002/ADTS.201900079
55. Hallab NJ, Bundy KJ, O'Connor K, Moses RL, Jacobs JJ. Evaluation of metallic and polymeric biomaterial surface energy and surface roughness characteristics for directed cell adhesion. *Tissue Eng*. 2001;7(1):55–70. doi:10.1089/107632700300003297
56. Tran TS, Dutta NK, Choudhury NR. Graphene inks for printed flexible electronics: graphene dispersions, ink formulations, printing techniques and applications. *Adv Colloid Interface Sci*. 2018;261:41–61. doi:10.1016/J.CIS.2018.09.003
57. Gao Y, Shi W, Wang W, Leng Y, Zhao Y. Inkjet printing patterns of highly conductive pristine graphene on flexible substrates. *Ind Eng Chem Res*. 2014;53(43):16777–16784. doi:10.1021/ie502675z
58. Saidina DS, Eawwiboonthanakit N, Mariatti M, Fontana S, Hérold C. Recent development of graphene-based ink and other conductive material-based inks for flexible electronics. *J Electron Mater*. 2019;48(6):3428–3450. doi:10.1007/s11664-019-07183-w
59. Soltman D, Subramanian V. Inkjet-Printed Line Morphologies and Temperature Control of the Coffee Ring Effect. *Langmuir*. 2008;24(5):2224–31. doi:10.1021/la7026847
60. Jiang C, Zhong Z, Liu B, et al. Coffee-ring-free quantum dot thin film using inkjet printing from a mixed-solvent system on modified ZnO transport layer for light-emitting devices. *ACS Appl Mater Interfaces*. 2016;8(39):26162–26168. doi:10.1021/ACSAMI.6B08679/SUPPL_FILE/AM6B08679_SI_001.PDF
61. Seifert T, Sowade E, Roscher F, Wiemer M, Gessner T, Baumann RR. Additive manufacturing technologies compared: morphology of deposits of silver ink using inkjet and aerosol jet printing. *Ind Eng Chem Res*. 2015;54(2):769–779. doi:10.1021/IE503636C/SUPPL_FILE/IE503636C_SI_001.PDF
62. Güngör GL, Kara A, Gardini D, Blosi M, Dondi M, Zanelli C. Ink-jet printability of aqueous ceramic inks for digital decoration of ceramic tiles. *Dyes Pigm*. 2016;127:148–154. doi:10.1016/J.DYEPIG.2015.12.018
63. Abel JS, Stangle GC, Schilling CH, Aksay IA. Sedimentation in flocculating colloidal suspensions. *J Mater Res*. 1994;9(2):451–461. doi:10.1557/JMR.1994.0451
64. Talbot EL, Yow HN, Yang L, Berson A, Biggs SR, Bain CD. Printing small dots from large drops. *ACS Appl Mater Interfaces*. 2015;7(6):3782–3790. doi:10.1021/AM5087177/SUPPL_FILE/AM5087177_SI_006.PDF
65. Liu L, Shen Z, Zhang X, Ma S. Low-temperature treatment for preservation and separation of graphene dispersions. *J Mater Sci*. 2018;53(19):13875–13885. doi:10.1007/S10853-018-2572-1
66. Mulla MA, Yow HN, Zhang H, Cayre OJ, Biggs S. Colloid Particles in Ink Formulations. *Fundamentals of Inkjet Printing*. 2016;141–168. doi:10.1002/9783527684724.CH6
67. Dou R, Wang T, Guo Y, Derby B. Ink-jet printing of zirconia: coffee staining and line stability. *J Am Ceram Soc*. 2011;94(11):3787–3792. doi:10.1111/J.1551-2916.2011.04697.X
68. Yao X, Peng R, Ding J. Cell–material interactions revealed via material techniques of surface patterning. *Adv Mater*. 2013;25(37):5257–5286. doi:10.1002/ADMA.201301762
69. Feng KC, Pinkas-Sarafova A, Ricotta V, et al. The influence of roughness on stem cell differentiation using 3D printed polylactic acid scaffolds. *Soft Matter*. 2018;14(48):9838–9846. doi:10.1039/C8SM01797B
70. Ross AM, Jiang Z, Bastmeyer M, Lahann J. Physical aspects of cell culture substrates: topography, roughness, and elasticity. *Small*. 2012;8(3):336–355. doi:10.1002/SMLL.201100934
71. Correia R, Deuermeier J, Correia MR, et al. Biocompatible parylene-C laser-induced graphene electrodes for microsupercapacitor applications. *ACS Appl Mater Interfaces*. 2022;14(41):46427–46438. doi:10.1021/ACSAMI.2C09667/SUPPL_FILE/AM2C09667_SI_001.PDF
72. Ferrari AC, Basko DM. Raman spectroscopy as a versatile tool for studying the properties of graphene. *Nat Nanotechnol*. 2013;8(4):235–246. doi:10.1038/NNANO.2013.46

73. Pastore Carbone MG, Beaugendre M, Koral C, et al. Thermoplastic polyurethane–graphene nanoplatelets microcellular foams for electromagnetic interference shielding. *Graphene Technol*. 2020;5(3–4):33–39. doi:10.1007/S41127-020-00034-0
74. Liao C, Li Y, Tjong SC. Graphene nanomaterials: synthesis, biocompatibility, and cytotoxicity. *Int J Mol Sci*. 2018;19(11):3564. doi:10.3390/IJMS19113564
75. Srikanth M, Khan W, Asmatulu R, Misak H, Yang S, Asmatulu E. In vitro cytotoxicity studies of industrially used common nanomaterials on L929 and 3T3 fibroblast cells. *J Biomed Res Environ Sci*. 2020;1(5):192–200. doi:10.37871/JBRES1143
76. Mirbagheri M, Adibnia V, Hughes BR, Waldman SD, Banquy X, Hwang DK. Advanced cell culture platforms: a growing quest for emulating natural tissues. *Mater Horiz*. 2019;6(1):45–71. doi:10.1039/C8MH00803E
77. Lin F, Du F, Huang J, et al. Substrate effect modulates adhesion and proliferation of fibroblast on graphene layer. *Colloids Surf B Biointerfaces*. 2016;146:785–793. doi:10.1016/J.COLSURFB.2016.07.008
78. Kumar S, Parekh SH. Linking graphene-based material physicochemical properties with molecular adsorption, structure and cell fate. *Commun Chem*. 2020;3(1):1–11. doi:10.1038/S42004-019-0254-9
79. Reddy S, Xu X, Guo T, Zhu R, He L, Ramakrishana S. Allotropic carbon (graphene oxide and reduced graphene oxide) based biomaterials for neural regeneration. *Curr Opin Biomed Eng*. 2018;6:120–129. doi:10.1016/j.cobme.2018.05.001
80. Zhu W, Ye T, Lee SJ, et al. Enhanced neural stem cell functions in conductive annealed carbon nanofibrous scaffolds with electrical stimulation. *Nanomedicine*. 2018;14(7):2485–2494. doi:10.1016/j.nano.2017.03.018
81. Lee JS, Lipatov A, Ha L, et al. Graphene substrate for inducing neurite outgrowth. *Biochem Biophys Res Commun*. 2015;460(2):267–273. doi:10.1016/J.BBRC.2015.03.023
82. Gurunathan S, Kim JH. Synthesis, toxicity, biocompatibility, and biomedical applications of graphene and graphene-related materials. *Int J Nanomed*. 2016;11:1927–1945. doi:10.2147/IJN.S105264
83. Ashok Sharma SS, Bashir S, Kasi R, Subramaniam RT. The significance of graphene based composite hydrogels as smart materials: a review on the fabrication, properties, and its applications. *FlatChem*. 2022;33:100352. doi:10.1016/J.FLATC.2022.100352